ELSEVIER

Fire Safety Journal **28** (1997) 351–378

0379-7112/97/$17·00
PII:0379-7112(97)00006-4

Fire Detection, Location and Heat Release Rate Through Inverse Problem Solution. Part II: Experiment

R. F. Richards, R. T. Ribail, A. W. Bakkom & O. A. Plumb

School of Mechanical and Materials Engineering, Washington State University, Pullman, WA 99164-2920, USA

(Received 22 February 1996; revised version received 20 November 1996; accepted 16 December 1996)

ABSTRACT

The design and fabrication of a prototype video fire detection system, which can locate a fire and determine its heat release rate, is described. The operation of the prototype system is demonstrated in a series of small-scale tests. The system utilizes a video camera to monitor an array of passive sensors distributed around the compartment to be protected. Each of the sensors is made up of a temperature-sensitive sheet that changes color at a prescribed temperature. In the event of an accidental fire, the plume of hot combustion gases rising from the fire will cause the temperature-sensitive sensors to be activated and change color. The times and locations of sensors changing color are used as data for an inverse problem solution algorithm, which determines the location and the heat release rate of the fire. A small-scale evaluation of the prototype video system is presented in which the prototype system is used to detect, locate and determine the heat release rate of a 2·4 kW burner placed in a 2·75 m wide by 2·75 m deep by 1·5 m high test enclosure. The accuracy of the prototype system in locating and determining the heat release rate of the small flame source placed in the reduced-scale enclosure is reported. In addition, the ability of the prototype system to make approximate measurements of the optical thickness of smoke in the enclosure, along camera-sensor lines-of-sight and then to use these measurements to locate and track the growth of a smoke plume is demonstrated. © 1997 *Elsevier Science Ltd.*

NOTATION

D	Optical depth from eqn (1)
d	Distance between sensors (m)
h	Height of ceiling (m)

h_c	Heating value of burner fuel ($kJ\,kg^{-1}$)
I	Intensity of laser beam passing through smoke-filled enclosure ($Wm^{-2}St^{-1}$)
I_o	Intensity of laser beam passing through smoke-free enclosure ($Wm^{-2}St^{-1}$)
$\dot{m}$	Mass flow rate of fuel in burner ($kg\,s^{-1}$)
Q_{act}	Actual fire heat release rate for flame source (W)
Q_{pred}	Fire heat release rate predicted by prototype fire detection system (W)
T_{amb}	Ambient temperature (K)
T_a	Sensor activation temperature (K)
(x_{act}, y_{act})	Actual flame source location (m)
(x_{pred}, y_{pred})	Flame source location predicted by prototype fire detection system (m)

Greek symbols

ΔT	$(T_a - T_{amb})$
ϵ_{loc}	Location error (m)
ϵ_Q	Heat release rate error ratio

1 INTRODUCTION

Fire detection systems are now being developed that not only can detect accidental fires, but can gather valuable information about the fire to aid in the suppression of the fire. These intelligent fire detection systems make use of the power of new microprocessor and sensor technologies to determine such information as the fire's location, the fuel feeding the fire and the rate of spread of the fire. The range of new sensor technologies being applied to fire detection is wide. For example Grosshandler and Jackson[1] describe the use of piezoelectric transducers to detect the acoustic emissions which are produced when structural elements in a building burn. Okayama[2] and Milke *et al.*[3] discuss the use of metal oxide sensors to detect the products of combustion produced in a fire. Falco and Debergh,[4] Brenci *et al.*[5] and Dubaniewicz *et al.*[6] explore the use of optical fibers to sense temperature fields, smoke and gas species associated with fire hazards such as CH_4 and CO. Noda and Ueda,[7] Nelson[8] and Healey *et al.*[9] deal with the use of color video technology, used in conjunction with either infrared or ultraviolet sensors to identify and locate fires. Ryser and Pfister[10] and Grosshandler[11] review recent developments in fire detection technology, especially in sensor technology and suggest possible directions for the future. In particular Grosshandler[11] proposes the development of

a fire detection system based on the use of a video camera to monitor passive, color-changing, temperature sensors. Work in our laboratory has led to the development of such a video-based fire detection system[12] that owes its intelligence to the application of inverse problem solution techniques.[13] The system locates an accidental fire and determines its heat release rate by solving the inverse heat transfer problem of the convective heating of a compartment ceiling by the plume of hot combustion gases produced by the fire.

The present paper describes the design, assembly and operation of a prototype video fire detection system which employs an inexpensive black and white video camera to monitor passive temperature-sensitive, color-changing sensors distributed around a compartment. The transient temperature data gathered by the video camera from the passive sensors is used in an inverse problem solution algorithm, implemented in a personal computer, to determine the fire's location and heat release rate.

Part I of this work,[13] focuses on the details of the inverse problem solution algorithm. In Part I, the theory behind the inverse problem solution algorithm is described and an evaluation of the inverse problem solution algorithm, based on both computer simulated and experimental data for fires in large enclosures is presented. In contrast, the present paper, Part II, focuses on the details of a working prototype of the video-based fire detection system. In Part II the hardware which makes up the prototype video fire detection system is described and an evaluation of the prototype fire detection system, based on small-scale fire experiments conducted in a reduced-scale enclosure is presented.

The design and assembly of the prototype video fire detection system is described first, with special attention paid to the passive sensors and the video system which monitors them. A laboratory-scale evaluation of the prototype system is presented next. The evaluation includes three series of tests. In the first series of tests, the ability of the video system to monitor the passive sensors and detect the activation of the temperature-sensitive, color-changing sensors is verified. In the second series of tests, the ability of the prototype system to detect a small flame source in a reduced-scale test enclosure and then to determine the location and the heat release rate of the flame source is tested. In the third series of tests, the ability of the prototype system to detect the presence of a smoke plume in the test enclosure and then to determine the location and the optical thickness of the smoke plume is evaluated.

It is important to note, that the three series of laboratory-scale tests making up the evaluation are not to be construed as an attempt to prove that the prototype video fire detection system is ready for full-scale implementation. On the contrary, the evaluation presented here is meant

only to demonstrate the concept of the video-based fire detection system and to test out its component parts on a small scale. It is intended that the evaluation based on large-scale simulated and experimental enclosure fires presented in Part I, will complement the evaluation based on small-scale tests presented here. While the present paper, Part II, demonstrates the operation of the video fire detection system on a small scale, Part I gives some indication of how the small-scale results would scale up to more realistic, large-scale applications.

2 SYSTEM DESCRIPTION

The operation of the video fire detection system is illustrated in Fig. 1. A black and white video camera monitors passive sensors placed in a regular array on the ceiling of the compartment to be protected. An accidental fire has ignited and begins to send a plume of hot smoke and combustion gases to the ceiling of the compartment. Each of the sensors is composed

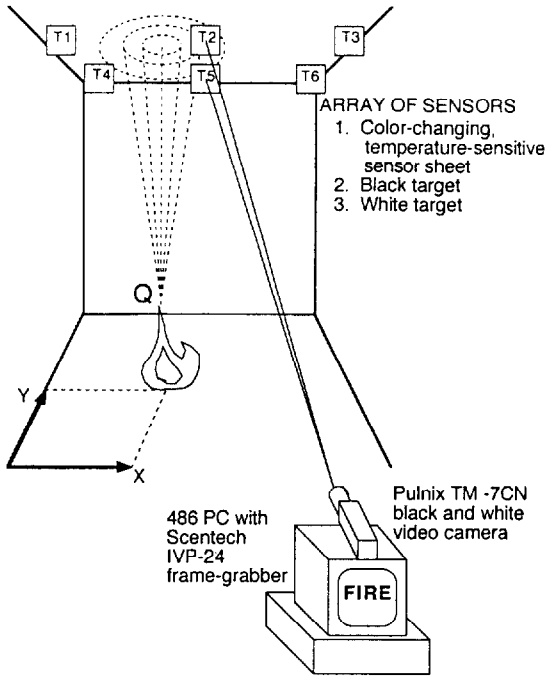

Fig. 1. The operation of the video fire detection system.

of a black target, a white target and a sheet of temperature-sensitive, color-changing material. Every sensor serves two functions. The temperature-sensitive material in the sensors visibly changes colour when the sensors reach their activation temperature. This color change enables the video system to track the advance of hot combustion gases across the ceiling. The black and white targets in the sensors serve as reference standards against which to measure the turbidity of smoke coming between the sensors and the video camera. Changes in the relative brightness of black and white targets on sensors obscured by smoke, enable the video system to track the advance of a fire's smoke plume. As sensors reach their activation temperature and change color, the video system records the location of the sensor and its time of activation. Once the temperature-sensitive material on five sensors has been activated, a personal computer based inverse problem solution algorithm uses those times of activation as data to determine the most probable location and heat release rate of the accidental fire.

The design of the video fire detection system can be best understood in terms of its two major components. The first major component is the video data gathering hardware, composed of the distributed array of sensors, the black and white video camera, and the frame grabber. The video data gathering hardware supplies the fire detection system with sensor time of activation data and line of sight optical density data. The second major component of the fire detection system is the personal computer based inverse problem solution algorithm which locates and sizes the fire.

2.1 Video data gathering hardware

The video camera used in the present work is a black and white Pulnex TM-7CN CCD camera equipped with a telephoto lens. Video images are digitized using a Scentech IV-P24 color frame grabber (using only one channel, for black and white images) and passed on to a 30 Mhz, 486 personal computer. This system is able to digitize and evaluate images from the video camera every 0·8 s, allowing for essentially continuous monitoring, The images digitized by the frame grabber and evaluated by the personal computer consist of 640×480 arrays of pixels with integer gray-scale values running from 0 (black) to 255 (white). Color changes in activated sensors appear in the digitized video images of sensors as changes in the gray-scale values of the pixels making up the images. To determine a color change in a sensor, the system calculates the average of the gray-scale values of twenty pixels in a sensor image. The choice of averaging over 20 pixels is a conservative measure and is taken to ensure

the elimination of errors due to electronic noise. A change in gray-scale of 15 out of 255 or 6% of the full gray-scale range is taken as the threshold value for sensor activation. The times of activation of the sensors are reckoned by reference to the personal computer's built in clock and are determined to the nearest second.

The sensors are 10×30 cm flat sheets composed of three, side by side, 10×10 cm areas: a black target, a white target and a temperature-sensitive, color-changing sheet. This sensor size is chosen so that sensor images are made up of at least 20 pixels, when camera to sensor distances are no more than 15 m. In systems requiring greater camera to sensor distances, larger sensors would be required, since the number of pixels that makes up a sensor image is proportional to the ratio of the linear dimensions of the sensor over the camera-to-sensor distance. For example, doubling the distance from camera to sensor to 30 m would require also doubling the linear dimensions of the sensors to 20×60 cm in order to ensure sensor images of at least 20 pixels.

Two kinds of temperature-sensitive materials are included in the tests of the sensors. The first batch of color-changing sheets is made by painting flat black paint on 0·1 mm thick plastic sheets and then painting over the black paint with a second coat of paint consisting of microencapsulated thermochromic liquid crystals (TLC) suspended in a clear binder. The TLC paint is transparent until it reaches the temperature of 30°C, so that the sheet appears black below 30°C. As the temperature of the TLC paint rises from 30 to 35°C the TLC paint selectively reflects light in a narrow wavelength band, with the wavelength band being a function of temperature. At 30°C the TLC paint reflects long wavelength light (red) and then reflects progressively shorter wavelength light until it reaches 35°C when blue is seen. As a result, the sensor appears to run through the colors of the visible spectrum. Above 35°C the TLC paint is again transparent and the sheet appears black. If the TLC paint is cooled from 35°C down to 30°C the colors of the spectrum are seen in reverse order, blue through red. Below 30°C the TLC paint reverts to its original appearance and is ready to be used again. The TLC color change is completely reversible, so that sensors fabricated with TLC paint can be activated many times.

A second batch of color-changing sheets is made by painting the same flat black paint on 0·1 mm plastic sheets and then painting over the black paint with a second coat of Omegalaq, a low-temperature melt paint material obtained from Omega Engineering Inc. Below its melting point at 38°C the melt paint is light purple. Upon melting the melt paint becomes semi-transparent, revealing the black undercoated paint. However, if the melt paint is heated above its melting point of 38°C and is then cooled below 38°C, the paint does not revert to its original appearance.

The melt paint color change is irreversible, so that sensors fabricated with melt paint can be activated only once.

All of the temperature sensors used in the present work have activation temperatures in the narrow band between 30 and 40°C. However, this range of activation temperatures is not a restriction imposed by the sensor materials employed. Both the TLC paint and the melt paint can be commercially obtained with activation temperatures ranging from below 0°C to over 100°C. As a result, temperature sensors can be fabricated with a wide range of activation temperatures and tailored to fit a variety of situations. For example, in situations where temperatures up to 40°C would routinely be expected, temperature sensors could be produced with activation temperatures of 45°C or greater.

In all sensors the black target is made by painting the same flat black paint on 0·1 mm plastic sheets. The appearance of the black target is thus identical to the TLC color-changing sheet before activation, and nearly identical to the melt paint color-changing sheet after activation. This equivalence in appearance allows sensor activation to be determined by comparing the average gray-scale pixel value of the temperature-sensitive, color-changing sensors against the gray-scale pixel value of the black target. The white targets are all cut from plain white poster board.

2.2 Inverse problem solution software

The development of the inverse problem solution algorithm is described in detail in Part I.[13] The algorithm is implemented in the event that the video data gathering system registers the color change, or activation of five adjacent sensors. As each sensor is activated, the personal computer records both the location and the activation time (clock time) of the sensor. Four elapsed times to activation are calculated for the second through the fifth sensors by subtracting their activation times from the activation time of the first sensor.

To determine the fire's location and heat release rate, the inverse problem solution algorithm compares the four measured activation times with activation times predicted by the zone fire model LAVENT[14] for various fire scenarios. More specifically, the algorithm calculates the sum of squares of differences between the measured activation times and predicted activation times computed by LAVENT for fires at various locations and with various growth rates. The fire scenario, or fire location and growth rate, which minimizes the sum of squares of the differences between measured and predicted times to activation is taken as representing the most probable fire location and growth rate.

In addition to describing the development of the inverse problem

solution algorithm, Part I also reports the results of an evaluation of the accuracy of the algorithm in determining fire location and growth rate in large-scale enclosures. In the evaluation, both computer synthesized fire data and data derived from experimental burns are used as input for the inverse problem solution algorithm. The evaluation demonstrates the limits of accuracy for the algorithm, given a range of levels of systematic model errors and random measurement errors.

3 PROTOTYPE SYSTEM EVALUATION

In order to demonstrate the underlying concepts behind the video fire detection system and to test the component parts of the system, an evaluation of a prototype system was undertaken. However, due to the lack of availability of full-scale experimental fire facilities, the evaluation of the prototype video fire detection system was restricted to tests that could be safely conducted in a reduced-scale enclosure. As a consequence the evaluation focused on issues which could be addressed in a series of small-scale tests: the ability of the video data gathering system to collect useable data from an array of sensors under conditions expected in a compartment fire (including the presence of smoke), the ability of the inverse problem solution algorithm to use data gathered by the video system to locate and size a small flame source and the ability of the fire detection system to locate a smoke plume. More specifically, the evaluation, was intended to answer three questions. First, could the video hardware continuously monitor an array of passive sensors and reliably detect either the activation of the temperature-sensitive sensors or the presence of smoke? Second, could the personal computer based inverse problem solution algorithm determine the location and heat release rate of a small flame source using for data only the sensor activation times supplied to it by the video hardware and do so quickly enough to make the system useful? Third, could the video system locate a smoke plume, track the plume, determine the plume's optical thickness, using for data only sensor gray-scale pixel values from video images supplied by the video hardware and do so in real time?

Answering these questions for a prototype system, on a small scale, is not sufficient to prove the efficacy of the proposed fire detection system in full-scale applications. However, proving the concept and the practicality of any proposed fire detection system on a small scale is a necessary condition that must be met before further investigation of the system on a large scale can be justified.

Three separate series of small-scale tests were conducted. The first

series of tests evaluated the ability of the video data gathering system to detect the activation of the temperature-sensitive, color-changing sensors under a range of lighting conditions and in the presence of smoke. In addition, the system's ability to detect smoke and to measure the optical density of the smoke was evaluated. The second series of tests evaluated the accuracy of the prototype video detection system in determining the location and heat release rate of 2·4 and 4·8 kW flame sources placed in a reduced-scale test enclosure. In these tests the inverse problem solution algorithm operated on data supplied to it by the video camera monitoring temperature-sensitive, color-changing sensors exactly as it would in an actual fire situation. The third series of tests evaluated the ability of the prototype system to make multiple, real-time, line-of-sight optical thickness measurements in order to determine the location and density of a smoke plume.

3.1 Sensor visibility and smoke detection

The ability of the video data gathering system to determine the activation of a temperature-sensitive, color-changing sensor was evaluated under a range of lighting conditions and smoke densities. To perform the evaluation a square array of nine sensors, spaced one meter apart, was suspended from the ceiling of a test enclosure. The sensors were numbered sequentially, left-to-right, in each row, beginning in the front row, as seen in Fig. 2. Both the reversible sensors fabricated with TLC

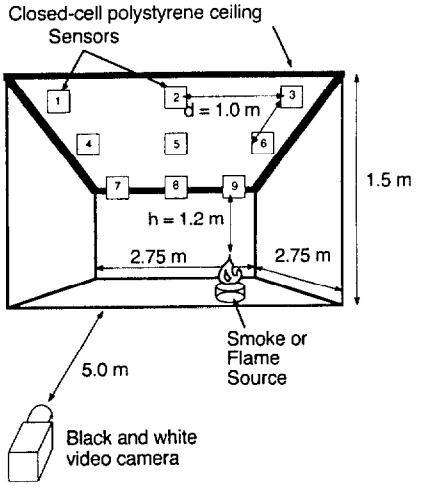

Fig. 2. The test enclosure.

paint and the irreversible sensors fabricated with the melt paint were tested. The test enclosure was 2·75 m deep, 2·75 m wide and 1·5 m high, or smaller than the ASTM standard fire test enclosure, which measures 3·7 m deep, 2·4 m wide and 2·4 m high.[15] The enclosure used in the present study, therefore, had a footprint 85% and a height 60% of the ASTM standard enclosure. The ceiling of the enclosure was constructed of 2·54 cm thick closed-cell polystyrene insulation. For test runs involving smoke, back and side walls constructed of heavy black plastic and a front wall of clear acrylic were installed. A fan connected to the rear of the test enclosure, near a bottom corner, exhausted through duct work leading out of the laboratory and was used to evacuate smoke from the test enclosure. For test runs without smoke, the back, side and front walls and the exhaust fan, were removed. During all tests, the monitoring video camera was placed outside the test enclosure, at a distance of about five meters, so that all nine sensors were visible simultaneously. This arrangement resulted in camera-to-sensor distances of between 5 and 8 m.

The effect of lighting on sensor visibility was evaluated by varying the level of illumination on the sensors. Illumination in the enclosure was controlled by turning on from one to nine 60 W incandescent light bulbs placed around the floor of the enclosure. Light levels on the sensors in the enclosure were measured with a hand held photographic light meter. Visibility of the sensors was quantified by averaging gray-scale values of pixels sampled from digitized sensor images.

The effect of smoke on sensor visibility and the ability of the video system to determine the optical density of smoke, were evaluated by measuring gray-scale pixel values of sensors obscured by known densities of smoke. The smoke was produced by a theatrical smoke machine.

A smoke machine was used in the tests because of concerns about repeatability in the experiments. First, the smoke machine was very consistent in its production of smoke from run to run. Second, the theatrical smoke left no residue or soot on the sensors after a run, ensuring that the sensors themselves did not change from run to run. In addition, the lack of sooting was important, because the motivation behind the tests was to isolate the effects of smoke on the visibility of the sensors. The presence of sooting on the sensors would have confounded the issue. Finally, the use of theatrical smoke as a surrogate for smoke from a real fire could be justified because the relationship between smoke optical density and visibility through smoke has been shown to be relatively insensitive to smoke composition.[16]

A test began by starting up the smoke machine and allowing the smoke to uniformly fill the test enclosure. Once the smoke had diffused out throughout the entire enclosure, the exhaust fan was turned on and the

smoke was slowly evacuated from the enclosure. The average gray-scale pixel values of the black target, the white target and the color-changing sheet in each sensor were recorded, as the smoke density decreased. At the same time as the gray-scale pixel values were determined, the optical density of the smoke in the enclosure was measured using light attenuation. The beam from a helium–neon laser was passed through the enclosure (3·66 m path length), and the intensity of the light which emerged was measured with a solid-state laser power meter. The optical density of the smoke, D, measured in decibels, was taken to be

$$D = -10 \log_{10} (I/I_o) \tag{1}$$

where I was the intensity of the laser beam after passing through the smoke-filled enclosure, and I_o, was the intensity of the laser beam after passing along the same path through the smoke-free enclosure.

3.2 Accuracy in fire location and heat release rate

The accuracy of the prototype fire detection system was evaluated in a series of small-scale tests by employing the fire detection system to detect, locate and size a small flame source placed in the reduced-scale enclosure test enclosure described earlier. The location and heat release rate of the flame source, as determined by the video fire detection system, was then compared to the actual location and heat release rate of the flame source.

For all test runs involving the flame source, the back, side and the front walls of the enclosure were removed, leaving the $2{\cdot}75 \times 2{\cdot}75 \times 1{\cdot}5$ m high enclosure open to the surrounding $9 \times 9 \times 3{\cdot}5$ m high laboratory. The ceiling of the enclosure, constructed of polystyrene insulation, served as an adiabatic surface. In this series of tests only the reversible sensors fabricated from the microencapsulated TLC paint were used. These color-changing, temperature-sensitive sensors had an activation temperature of $T_a = 33$°C. The flame source used was a backpacker's camp stove which burned unleaded gasoline in a premixed flame. The height of the burner and its stand was approximately 0·30 m, giving a distance of 1·20 m from the burner flame to the enclosure ceiling. The thermal output of the burner was estimated to be $Q_{act} = 2{\cdot}4 \pm 0{\cdot}3$ kW, by measuring the mass flow of fuel in the stove, $\dot{m} = 5{\cdot}0 \pm 0{\cdot}3 \times 10^{-5}$ kg s^{-1}, and multiplying by an estimate of the heating value of the fuel, $h_c = 4{\cdot}8 \pm 0{\cdot}4 \times 10^3$ kJ kg^{-1}. The contributions to uncertainty in Q_{act}, due to incomplete combustion and radiation from the flame were very small compared to the contributions due to uncertainties in the mass flow rate and heating value of the burner fuel.

A test run was started by activating the prototype video fire detection

system. The video system determined the status of all nine sensors in the test enclosure every 0·8 s. With the fire detection system operating, the burner was ignited and placed under the sensor array in the enclosure. As sensors were activated by the plume of hot gases rising from the flame source, the temperature-sensitive sheets changed color. As color changes were detected by the video system, the personal computer would record the location of the activated sensor and the sensor's time of activation. Once five sensors had been activated, and their color change detected, the personal computer would call the inverse problem solution algorithm. The algorithm would then take less than 2 s to determine the most probable location and heat release rate of the flame source.

To quantify system accuracy, the actual location and heat release rate of the camp stove flame source was compared to the location and heat release rate determined by the prototype system. Location error, ϵ_{loc}, was calculated from

$$\epsilon_{loc} = \sqrt{(x_{pred} - x_{act})^2 + (y_{pred} - y_{act})^2} \tag{2}$$

where (x_{act}, y_{act}) was the actual location of the camp stove and (x_{pred}, y_{pred}) was the prototype system's prediction of the location of the camp stove. Heat release rate error ratio, ϵ_Q, was calculated from

$$\epsilon_Q = Q_{pred}/Q_{act} \tag{3}$$

where Q_{pred} was the prototype system's estimate of the camp stove's heat release rate and Q_{act} was the actual heat release rate of the camp stove given above.

3.3 Smoke plume location

The ability of the video fire detection system to determine the location of a smoke plume was evaluated. Smoke plume location tests were made with the side walls and front window of the enclosure in place, but with the exhaust fan turned off. A test run began by activating the prototype fire detection system. The smoke machine was placed under the sensor array, at a set location on the floor in the enclosure. When the smoke machine was started up, it produced a well-defined plume of smoke that rose to the ceiling and then turned, spreading out as a ceiling jet and filling the enclosure. As the smoke plume rose and filled the test enclosure, the average gray-scale pixel values of the digitized images of each of the nine sensors were recorded. Using the calibration curves for smoke density developed during the sensor visibility and smoke detection tests, the measured gray-scale pixel values for the black and white targets were converted into estimated optical thicknesses along each camera-to-sensor

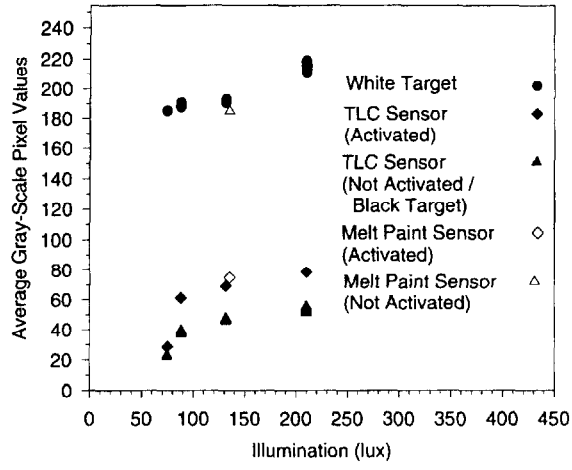

Fig. 3. Average gray-scale values of sensor images versus illumination.

line of sight. Those line of sight optical thicknesses were then used to establish the location and density of the smoke plume.

4 RESULTS

4.1 Sensor visibility and smoke detection

The effect of the level of illumination on sensor visibility is shown in Fig. 3. In that figure gray-scale pixel values of digitized sensor images taken by the prototype video fire detection system are plotted against the level of illumination on the sensors. Illumination is given in units of lux. Gray-scale pixel values are given as integer values from 0 to 255, since the frame-grabber is an eight-bit device. The value 0 represents the lowest level of brightness (black) while 255 represents the highest level of brightness (white). The figure shows average digitized gray-scale values for each of the black and white targets, and the temperature-sensitive, color-changing sheets (TLC and melt paint sheets), before and after activation. Recall that the black target was identical in appearance to the TLC temperature-sensitive, color-changing sheet before activation, and nearly identical to the melt paint sheet after activation.

Gray-scale values for the black and white targets and the activated TLC sheets are all seen to increase as illumination levels rise from 75 to 210 lux. The increase is greatest for the black target and the activated TLC sheet

at illumination levels less than 100 lux. At higher illumination levels the increase in gray-scale pixel values of the black target and activated TLC sheet are small. The gray-scale pixel values of the white target increases slowly at all levels of illumination.

Of more importance is the change in gray-scale values of the TLC sensor upon activation because it is this difference which must be detected to determine the TLC sensor activation. Figure 3 shows that the difference between gray-scale pixel values of unactivated TLC sheets (black target) and activated TLC sheets also grows as illumination increases. Below 90 lux the difference between activated and unactivated TLC sheets is extremely small, less than 10 or 4% of the full gray-scale range. Between 90 and 100 lux the difference in gray-scale pixel values of activated and unactivated TLC sheets rises sharply to 25 or 10% of the full gray-scale range. For levels of illumination above 100 lux, the difference in gray-scale values between activated and unactivated TLC sheets grows very slowly. In this plateau region, the detection of sensor activation will not be affected by changes in the level of illumination.

The small change in gray-scale pixel value upon activation, means that detecting the activation of TLC sheets is relatively difficult. Sensors based on melt paint sheets display a greater change upon activation. Figure 3 shows the average gray-scale pixel values for a sensor with a melt paint temperature-sensitive sheet, before and after activation, at one level of illumination, 140 lux. Before activation, the melt paint sheet is light in color, with an average gray-scale pixel value of 185. After activation the melt paint becomes semi-transparent, revealing the black undercoat beneath. The activated melt paint sensor has a gray-scale value of 75, close to the black target gray-scale value of 70 at the same illumination. The change in gray-scale value upon activation of the melt paint sensor is quite large: 110 or more than 40% of the full gray-scale range. As a consequence, the use of this kind of temperature-sensitive, color-changing material produces a more robust sensor.

The effect of smoke on the visibility of the temperature-sensitive, color-changing TLC sheets is illustrated in Fig. 4. In the figure, the difference in gray-scale pixel values for a TLC sensor before and after activation are plotted against the optical density of smoke (in units of decibels) filling the test enclosure. The change in gray-scale values of the TLC sensor upon activation, is seen to decrease linearly from 25 or 10% of full gray-scale range to a value of 15, or 6% of full range as smoke optical density increases from 0 to 7 db. To function under smoky conditions typical of a fire environment, the prototype video system must be capable of detecting changes of gray-scale values less than 15.

Figure 5 shows the effect of smoke on the visibility of the black and

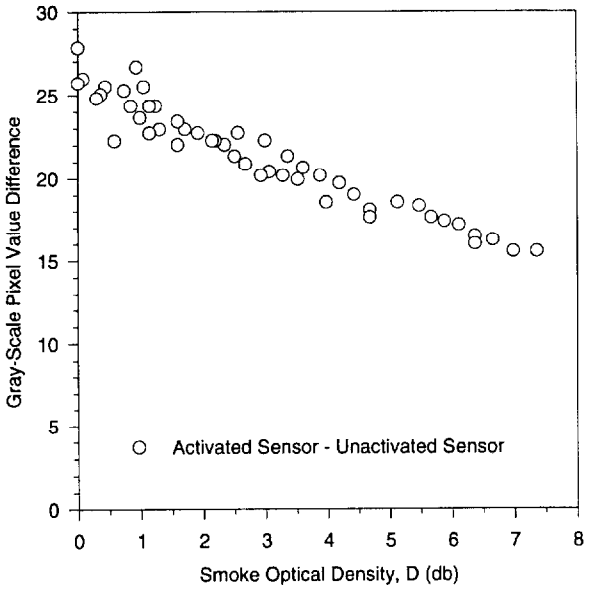

Fig. 4. Visibility of TLC sensor activation: difference between gray-scale pixel values of activated and unactivated sensors versus smoke optical density.

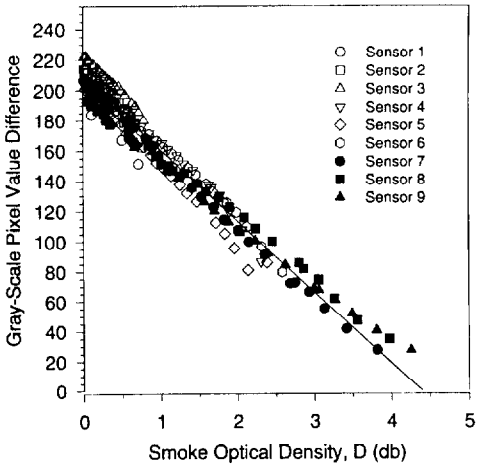

Fig. 5. Smoke obscuration of black and white targets: difference between gray-scale pixel values of black and white targets versus smoke opical density.

white targets in each sensor. In the figure, the difference between the average gray-scale pixel values of the black and white targets versus the optical density of smoke between the targets and the video camera is plotted. Data are shown for all nine sets of black and white targets. The difference in gray-scale pixel values of the black and white targets decreases linearly as smoke optical density increases, just as the difference in gray-scale values for the TLC sheets did. However, the difference between the black and white targets is much larger than that for the TLC sensors. The difference between black and white target gray-scale values falls from a high of 210 (80% of full range) at 0 db to a low of 30 (10% of full range) at 4 db. The data for all nine sensors are seen to lie in a narrow band.

The large change in black and white target gray-scale values for the entire range of smoke optical densities seen in Fig. 5, means that the prototype fire detection system is able to detect small concentrations of smoke. The linear relationship between the black and white target gray-scale values and the smoke optical density, seen in Fig. 5, means that the prototype video fire detection system can be calibrated to make useful smoke optical density measurements along camera-to-sensor lines-of-sight.

4.2 Accuracy in fire location and heat release rate

The accuracy of the prototype video fire detection system in determining the location and heat release rate of a small flame source in the reduced-scale enclosure can be judged by referring to Figs 6–8. The figures show probability density functions (pdfs) for the prototype video fire detection system's location errors and heat release rate error ratios, as measured for experimental runs conducted in the reduced-scale test enclosure using the small 2·4 kW burner as a flame source.

In all experimental runs, the time to activation for five sensors, was never more than 50 s. With the additional 2 s required to run the inverse problem solution algorithm, the time from ignition of the small flame source to the determination of the burner's location and heat release rate by the prototype fire detection system, in the more than 200 small-scale test burns conducted, was never more than 1 min.

Figure 6(a) gives the pdf for system location error and Fig. 6(b) gives the pdf for system heat release rate error ratio for 100 trials of the prototype system. All trials were conducted with the sensor spacing set at $d = 1{\cdot}00$ m, the difference between sensor activation temperature and ambient temperature held constant at $\Delta T = 11°C$ ($T_a = 33°C$, $T_{amb} = 22°C$) and the flame source heat release rate at $Q_{act} = 2{\cdot}4$ kW.

The prototype video fire detection system is seen to have determined

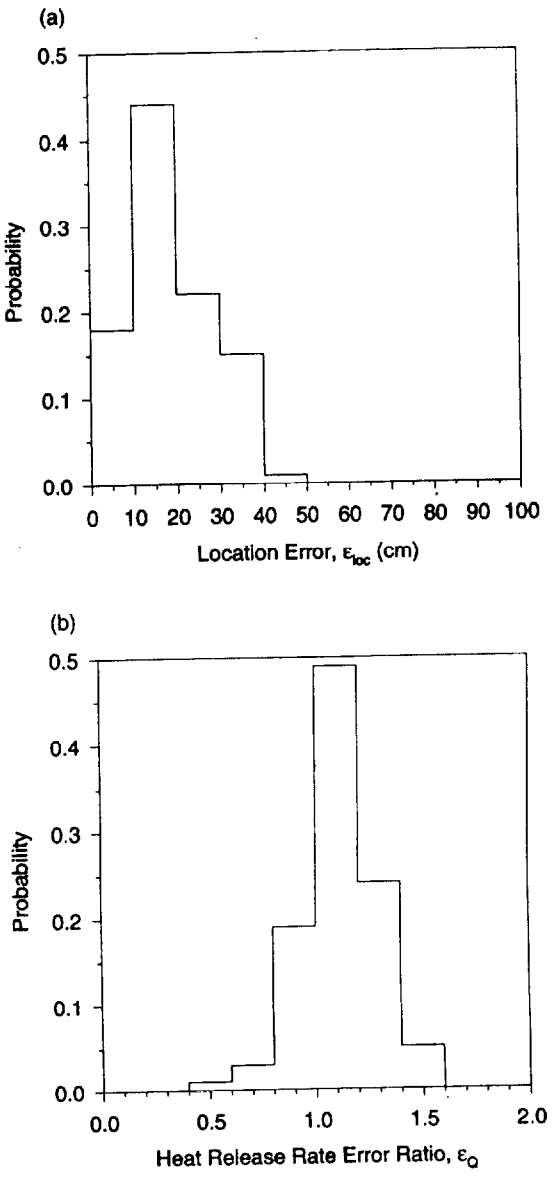

Fig. 6. (a) Location error pdf for 100 trials at standard conditions: $d = 1{\cdot}00$ m, $\Delta T = 11°C$, $Q_{act} = 2{\cdot}4$ kW. (b) Heat release rate error ratio pdf for 100 trials at standard conditions: $d = 1{\cdot}00$ m, $\Delta T = 11°C$, $Q_{act} = 2{\cdot}4$ kW.

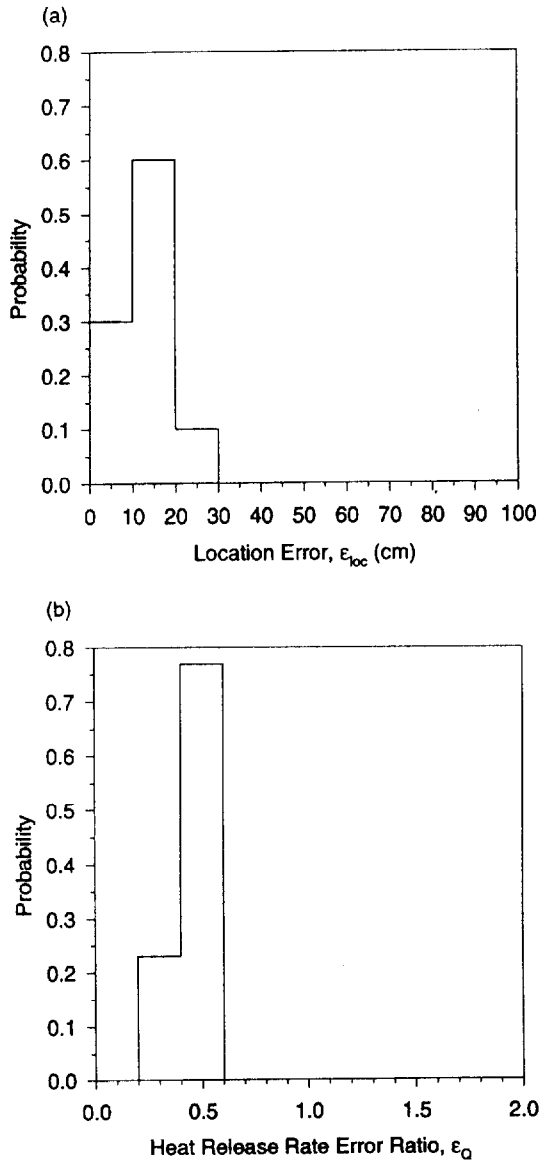

Fig. 7. (a) Location error pdf for 30 trials at reduced sensor spacing: $d = 0{\cdot}50$ m, $\Delta T = 11$°C, $Q_{act} = 2{\cdot}4$ kW. (b) Heat release rate error ratio pdf for 30 trials at reduced sensor spacing: $d = 0{\cdot}50$ m, $\Delta T = 11$°C, $Q_{act} = 2{\cdot}4$ kW.

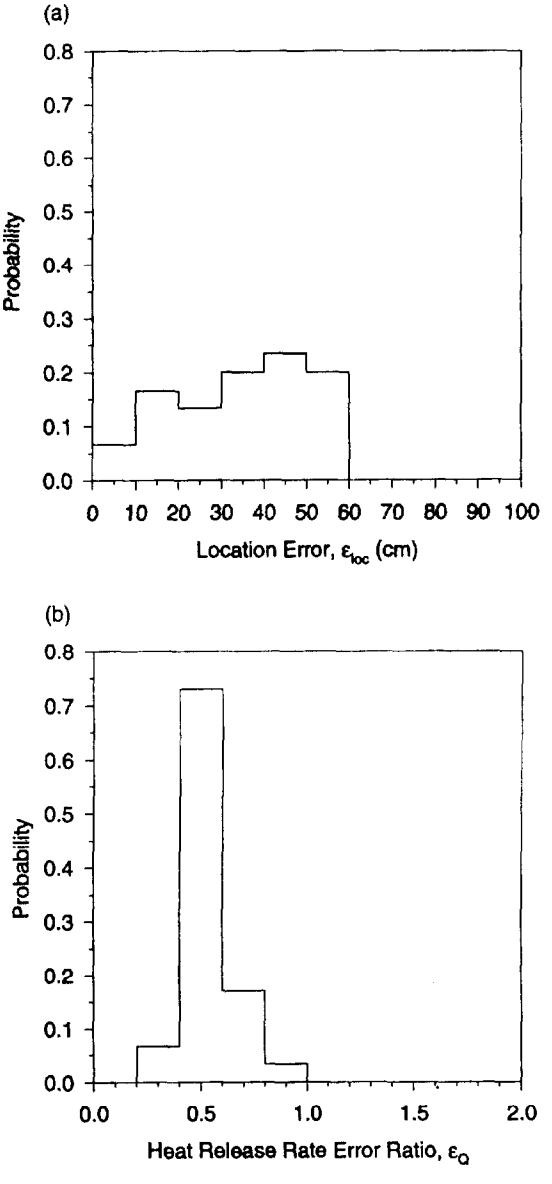

Fig. 8. (a) Location error pdf for 30 trials at reduced difference between sensor activation temperature and ambient temperature: $d = 1{\cdot}00$ m, $\Delta T = 6$°C, Q_{act}-2·4 kW. (b) Heat release rate error ratio pdf for 30 trials at reduced difference between sensor activation temperature and ambient temperature: $d = 1{\cdot}00$ m, $\Delta T = 6$°C, $Q_{act} = 2{\cdot}4$ kW.

the location of the flame source in all 100 trials to within 0·50 m or to within one-half of the sensor spacing ($d/2$). The mean location error is much less, about 0·20 m, or $d/5$. Heat release rate error ratios for the 100 trials of the prototype system are seen to lie between the values of $\epsilon_Q = 0{\cdot}4$ and 1·6. In every test run the prototype system was able to determine the heat release rate of the 2·4 kW flame source to within ±60%. The mean heat release rate error ratio is $\epsilon_Q = 1{\cdot}1$, very close to a value of unity. The heat release rate error ratios for the majority (about 70%) of the test runs lie in the range $\epsilon_Q = 0{\cdot}8$–1·2. In other words, the heat release rate of the flame source was predicted within ±20% for most test runs.

Figure 7(a,b) demonstrates the effect of sensor spacing, d, on the accuracy of the prototype video system. Figure 7(a) gives the location error pdf and Fig. 7(b) gives the heat release rate error ratio pdf for 30 trials in which the sensor spacing was reduced to $d = 0{\cdot}50$ m. The difference between sensor activation temperature and ambient temperature was unchanged at $\Delta T = 11°C$ ($T_a = 33°C$, $T_{amb} = 22°C$) and the flame source heat release rate was $Q_{act} = 2{\cdot}4$ kW, as in the previous set of test runs.

The pdfs in Fig. 7(a,b) shows that reducing the sensor spacing, d, causes absolute values of fire location errors to decrease. However, the decreased sensor spacing, d, causes fire location errors normalized by the sensor spacing, d, to increase and errors in predictions of fire heat release rate to increase. Location errors for all thirty runs are all less than $\epsilon_{loc} = 0{\cdot}30$ m, or just over $d/2$, while the mean location error is about $\epsilon_{loc} = 0{\cdot}15$ m or just under $d/3$. Heat release rate error ratios for the 30 trials range from $\epsilon_Q = 0{\cdot}2$ to 0·6, with a mean value of $\epsilon_Q = 0{\cdot}45$. In this case, with reduced sensor spacing, the prototype fire detection system underestimates the heat release rate of the flame source in all trials and on average underestimated heat release rate by a factor of two.

Figure 8(a,b) shows the effect of the difference between sensor activation temperature and ambient temperature, $\Delta T = (T_a - T_{amb})$, on the accuracy of the prototype video system. Figure 8(a) gives the location error pdf and Fig. 8(b) gives the heat release rate error pdf for 30 trials in which the difference between activation and ambient temperatures is reduced to $\Delta T = 6°C$ ($T_a = 33°C$, $T_{amb} = 26°C$). In all trials the sensor spacing was $d = 1{\cdot}00$ m, and the flame source heat release rate was $Q_{act} = 2{\cdot}4$ kW.

The pdfs in Fig. 8(a,b) show that decreasing the temperature difference causes errors in predictions of both fire location and fire heat release rate to increase. In particular, for one-fifth of the trials (6 out of 30 trials), location errors are greater than $\epsilon_{loc} = 0{\cdot}50$ m, or more than $d/2$. The

mean location error is $\epsilon_{loc} = 0{\cdot}35$ m or about $d/3$. The prototype system underpredicts the heat release rate of the flame source in all 30 trials. Heat release rate error ratios for the 30 trials lie in the range from $\epsilon_Q = 0{\cdot}2$–$1{\cdot}0$, with a mean value of $\epsilon_Q = 0{\cdot}55$.

Figure 9(a,b) shows the result of doubling the heat release rate of the flame source to $Q_{act} = 4{\cdot}8$ kW, from the value of $Q_{act} = 2{\cdot}4$ kW used in earlier tests. The larger heat release rate was produced by placing two 2·4 kW burners side by side in the test enclosure. Figure 9(a) gives the location error pdf and Fig. 9(b) gives the heat release rate error ratio pdf for 30 trials. The sensor spacing was $d = 1{\cdot}0$ m and the difference between sensor activation and ambient temperature was $\Delta T = 11°C$.

The location error pdf in Fig. 9(a) is wider than for any previous case, ranging up to $\epsilon_{loc} = 0{\cdot}70$ m. The mean location error is $\epsilon_{loc} = 0{\cdot}30$ m or about $d/3$. Once again, the heat release rates determined by the prototype system are seen to be low, although not as low as in previous cases. Heat release rate error ratios range from $\epsilon_Q = 0{\cdot}4$–$1{\cdot}0$. The mean heat release rate error ratio is $\epsilon_Q = 0{\cdot}7$

The behavior seen in Figs 7–9 can be understood by considering how the ratio of the magnitude of error in the sensor activation times to the magnitude of the sensor activation times changes in each set of trials. In each of the pair of figures, the effect of sensor spacing, d (Fig. 7(a,b)), the difference between activation and ambient temperatures, ΔT (Fig. 8(a,b)) and the heat release rate of the flame source, Q_{act}, (Fig. 9(a,b)) is to cause activation times to decrease while the errors associated with the activation times remain constant. As shown in Part I,[13] it is this ratio of activation time error to activation time and not the absolute magnitude of the error which controls the accuracy of the inverse problem solution algorithm.

In Fig. 7(a,b), reducing the sensor spacing, d, causes sensor activation times to be reduced, while not affecting the error associated with the measured sensor activation time. As a result, reducing sensor spacing causes the ratio of activation time error to activation time to increase. The increase in this ratio results in the increase in heat release rate errors seen in Fig. 7(b). In contrast, the absolute location errors seen for the reduced sensor spacing in Fig. 7(a) are smaller than those seen in Fig. 6(a). However, the location error normalized by sensor spacing increases as sensor spacing increases. Recall that in Fig. 6(a), where $d = 1{\cdot}00$ m, the mean location error is about $d/5$ while in Fig. 7(a), where $d = 0{\cdot}50$ m, the mean location error increases to $d/3$.

In Fig. 8(a,b), reducing the difference between activation and ambient temperatures, ΔT, causes sensor activation times to be reduced, without affecting the error in activation time measurements, just as in Fig. 7(a,b) when sensor spacing, d, was reduced. Reducing ΔT, increases the ratio of

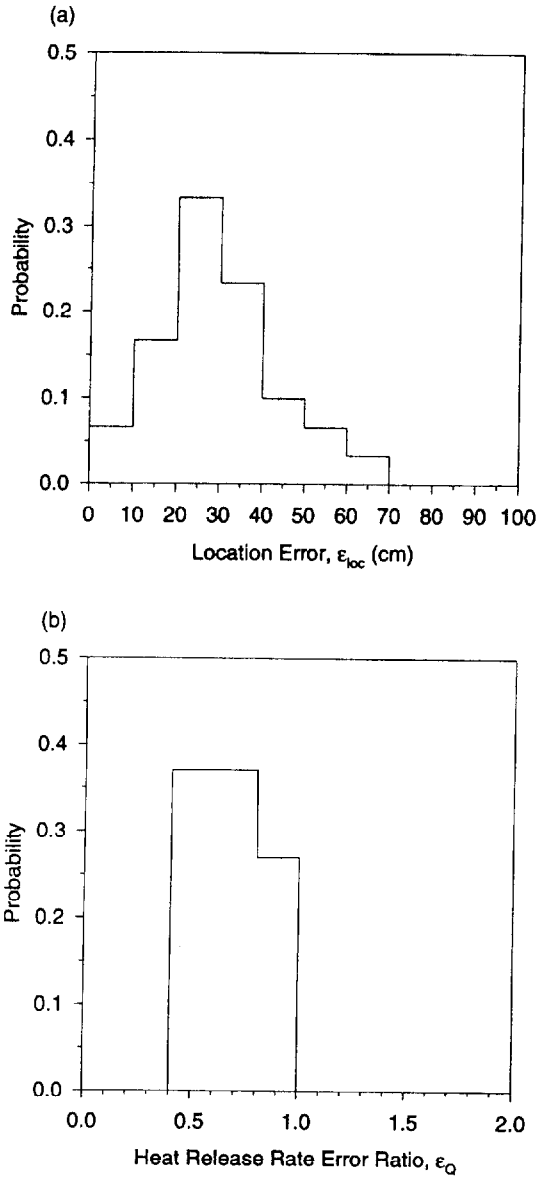

Fig. 9. (a) Location error pdf for 30 trials at increased heat release rate: $d = 1{\cdot}00$ m, $\Delta T = 11°C$, $Q_{act} = 4{\cdot}8$ kW. (b) Heat release rate error ratio pdf for 30 trials at increased heat release rate: $d = 1{\cdot}00$ m, $\Delta T = 11°C$, $Q_{act} = 4{\cdot}8$ kW.

activation time error to activation time, just as reducing sensor spacing, d, did. The result is an increase in both location error and heat release rate error for the prototype system. In addition, the increases in location error and heat release rate error are similar in magnitude to those seen in Fig. 7(a,b), when sensor spacing was reduced. In both cases the mean location error increases to $d/3$ and the mean heat release rate error ratio falls to about one-half.

In Fig. 9(a,b), increasing the heat release rate of the flame source, Q_{act}, causes sensor activation times to be reduced, without affecting the error in activation time measurements. Once again the increased errors in fire location and heat release rate predictions seen in Fig. 9(a,b) can be attributed to the increase in the ratio of activation time error to activation time. In this case, however, the increase in location error is larger than the increase in heat release rate error. The greater increase in location errors can be attributed, in part, to the fact that two burners were used together to make up the flame source. These two burners could not be placed closer to one another than about 0·20 m (center-to-center). The fire model used in the inverse problem solution algorithm is limited by an assumption of a point source for the fire plume and does not have the capability to model two interacting plumes. As a consequence, it is not surprising that the predictions of the inverse algorithm degrade under these conditions.

The significance of the ratio of the activation time error to the activation time appears to be independent of the scale of the inverse fire detection problem. The effect of scale on these results and the significance of the ratio of activation time error to activation time, can be judged by comparing the present results with those results reported in Part I.[13] In Part I, evaluations of the inverse problem solution algorithm using both computer synthesized data and data interpolated from experimental measurements were presented for compartment fires on a much larger scale than the experiments presented above. In Part I, the evaluations involved a compartment measuring $20 \times 20 \times 3$ m high, and fires with heat release rates as large as 100 kW, compared to the small-scale experiments with 2·4 and 4·8 kW flame sources in a $2{\cdot}75 \times 2{\cdot}75 \times 1{\cdot}5$ m high enclosure presented above. Two comparisons can be made between the results of these previous large-scale tests to the present small-scale tests.

First, in the evaluation based on computer synthesized fire data presented in Part I, the ratio of activation time error to activation time was shown to be the controlling parameter in fire location and heat release rate errors. This result was seen in the larger location and heat release rate errors for fast-growing fires than for slow-growing fires, even when systematic and random errors did not change. Fast-growing fires had

shorter sensor activation times than slow-growing fires, so that when systematic and random errors were constant, the ratio of activation time error over activation time increased. The same result is shown in Figs 7–9.

Second, the magnitude of errors found in the evaluation in Part I, based on data interpolated from large-scale experimental test burns are very similar to the magnitude of errors found in the small-scale experiments and presented in Figs 6–9 above. In the evaluation from Part I, the inverse problem was found to locate 95% of all fires within $2/3d$ and 50% of all fires within $d/3$, while determining the heat release rate of 95% of all fires within a factor of five and 50% of all fires within a factor of three. Those results can be compared to the results found for the 190 experimental runs in the reduced-scale enclosure presented above. In the small-scale tests of the video fire detection system, which utilized the same inverse problem solution algorithm as in Part I, the prototype system was able to locate all fires within $2/3d$ and 50% of all fires within $d/3$, while determining the heat release rate of all fires within a factor of five and 50% of all fires within a factor of between two and three.

4.3 Smoke plume location

The ability of the prototype video fire detection system to detect smoke and determine the optical density of the smoke has already been discussed. Recall that Fig. 5 showed that the difference between gray-scale pixel values of black and white targets could be correlated against the optical density of smoke along the line of sight between the sensor and the video camera. As a consequence, the availability of simultaneous line of sight optical density measurements from the camera to several sensors enables the system to track the location of a spreading smoke plume. Figure 10 shows how a smoke plume can be detected, located and tracked over time.

As described earlier, a smoke plume was created by a smoke generator placed in the enclosure. Figure 10 shows results when the smoke generator was placed below sensor four, located at the far left of the second row (position (2,3) in the figure). The figure represents line-of-sight optical density measurements for the nine sensors in the enclosure, at four elapsed times after the initiation of the smoke plume. Figure 10(a,b,c,d), respectively, shows the line-of-sight optical density measurements after 8, 12, 16 and 20 s had elapsed. Before 8 s no sign of the smoke can be detected. The arrival of the smoke plume at the ceiling of the enclosure is apparent after 12 s. Between 16 and 20 s the smoke thickens in the vicinity of sensor four and the plume begins to spread obscuring sensors five and

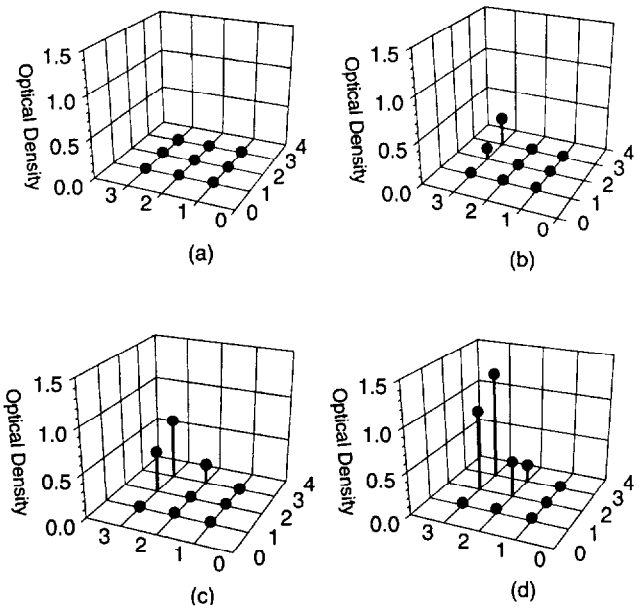

Fig. 10. Line of sight optical density measurements for all nine sensors in the test enclosure, during the growth of a smoke plume from a smoke generator placed under sensor four, at location (2,3): (a) $t = 8$ s, (b) $t = 12$ s, (c) $t = 16$ s, and (d) $t = 20$ s.

eight. Subsequent measurements showed the plume filling the entire ceiling of the enclosure.

The very short time scales required to detect the smoke and track the plume indicates that soot deposition on the sensors should not pose a significant problem for the video fire detection system. Even a very sooty smoke plume could not deposit much soot on the sensors in the twenty seconds represented by Fig. 10. While later smoke optical density measurements by the video system would be in error if soot accumulated on the sensors, this error would not affect the goal of the video fire detection system: the early detection and location of the smoke plume.

5 CONCLUSIONS

A prototype fire detection system, employing a video camera to monitor an array of temperature-sensitive, color-changing sensors and an inverse problem solution algorithm to determine the location and heat release rate of an accidental fire has been described. The operation of the

prototype fire detection system can be understood in terms of its two major components: the video data-gathering hardware and the inverse problem solution software.

The video data-gathering hardware consists of an array of color-changing, temperature-sensitive sensors, a video camera which monitors them and a frame grabber which digitizes the video images and passes them on to a personal computer. The inverse problem solution software consists of a personal computer based FORTRAN algorithm, which uses the times of activation of five of the ceiling mounted sensors gathered by the video hardware to determine the most probable location and heat release rate of an accidental fire.

Two candidate (commercially available) temperature-sensitive, color-changing materials were evaluated: a thermochromic liquid crystal (TLC) paint and a temperature-indicating melt paint. The color change of sensors fabricated with the TLC paint was shown to be detectable by the video camera used in the present study, at illumination levels as low as 100 lux and through smoke with optical density as great as 7 db. However, the change in gray-scale value of the TLC sensors upon activation was small. In contrast the change in gray-scale value of sensors fabricated from the melt paint was much greater. As a consequence, sensors fabricated with the temperature-indicating melt paint would be significantly easier to monitor than the TLC sensors. The temperature-indicating melt paint sensors do have the drawback of being irreversible and, therefore, less convenient to use.

The accuracy of the prototype video fire detection system in determining the location and heat release rate was evaluated in a series of small-scale tests, involving a 2·4 kW burner used as a flame source in a reduced-scale enclosure. In an initial set of 100 test runs, the prototype system was able to locate the flame source to within one-half the sensor-to-sensor spacing, $d/2$, for all test runs and to within one-fifth of the sensor-to-sensor spacing, $d/5$, for most of the test runs. In the same set of 100 trials, the prototype system was able to determine the heat release rate of the flame source in all test runs to within a factor of three, and to determine the heat release rate of the flame source in most test runs to within 20%. In addition to the inital 100 test runs another 90 small-scale tests were run in which sensor spacing, d, the difference between ambient and sensor activation temperatures, ΔT, and the flame source's heat release rate, Q_{act}, were varied to determinine the effect of those parameters on the prototype system's ability to predict the location and heat release rate of the flame source. When those 90 test runs were considered together with the initial 100 test runs, the prototype system was shown to have located all fires within $2/3d$ and 50% of all fires within

$d/3$, while determining the heat release rate of all fires within a factor of five and 50% of all fires within a factor of three. The location and heat release rate errors found in these 190 small-scale experimental tests were very close to the results of the large-scale evaluations of the inverse problem solution algorithm presented in Part I of this work.

The accuracy of the inverse problem solution algorithm was seen to depend on the ratio of the magnitude of errors in measured sensor activation times to those activation times. Increasing this ratio by reducing the sensor spacing, d, reducing the difference between ambient and sensor activation temperatures, ΔT, or increasing the flame source's heat release rate, Q_{act}, caused increases in both location and heat release rate errors. The ratio of the sensor activation time errors to the sensor activation time was, thus, shown to be as important in the small-scale tests presented here, as it was in the large-scale evaluations in Part I.

The ability of the prototype video system to make approximate optical thickness measurements along camera-to-sensor lines of sight was evaluated. Gray-scale pixel value measurements from video images of black and white targets on the array of sensors were calibrated against optical thickness as measured by laser light attenuation. The ability of the system to use these line of sight optical thickness measurements to locate a smoke plume and track its growth was demonstrated.

ACKNOWLEDGEMENTS

This work has been supported by the Building and Fire Research Laboratory of NIST through contract number 60NANB2D1290, Dr W.L. Grosshandler, scientific officer. The assistance of WSU undergraduate research assistant, C. Wark, in gathering data during the evaluation of the prototype fire detection system is gratefully acknowledged.

REFERENCES

1. Grosshandler, W. L. & Jackson, M., *Fire Safety Journal*, **22**(3) (1994) 209–228.
2. Okayama, Y., *Third International Symposium of Fire Safety Science*, 1991, pp. 955–964.
3. Milke, J. A., Hagen, B. C., McAvoy, T. J. & Pan, D., NISTIR 5499. National Institute of Standard and Technology, Gaithersburg, MD, 1994.
4. Falco, L. & Debergh, P., AUBE '89, University of Duisburg, Germany, October 1989.
5. Brenci, M., Guzzi, D., Mencaglia, A. & Grazia, A., *Measurement*, **12**(2) (1993) 183–190.

6. Dubaniewicz, T. H., Chilton, J. E. & Dobroski, H., *IEEE Transactions on Industry Applications*, **29**(4) (1993) 749–754.
7. Noda, S. & Ueda, K., *Proceedings of the* 1994 *Vehicle Navigation and Information Systems Conference, IEEE*, Yokohama, Japan, August 1994, pp. 57–62.
8. Nelson, D. F., *Annual Conference on Fire Research: Book of Abstracts*. National Institute of Standards and Technology, Gaithersburg, MD, 1993.
9. Healey, G., Slater, D., Lin, T., Drda, B. & Goedeke, A. D., *IEEE Computer Vision and Pattern Recognition Proceedings of the* 1993 *IEEE Computer Society Conference on Computer Vision and Pattern Recognition*, New York, June 1993, pp. 605–6.
10. Ryser, P. & Pfister, G., *Transducers* '91, 1991 *International Conference on Solid-State Sensors and Actuators*, San Francisco, CA, June 1991, pp. 579–583.
11. Grosshandler, W. L., *Heat and Mass Transfer in Fire and Combustion Systems*, HTD-Vol. 223, 1992, pp. 1–10.
12. Richards, R. F., Munk, B. N., Plumb, O. A. & Grosshandler, W. L., *Proceedings of the* 10*th International Conference on Automatic Fire Detection, AUBE* '95, Duisburg, Germany, 1995.
13. Richards, R. F., Munk, B. N. & Plumb, O. A., *Fire Safety Journal*, **28**(4) (1997) 323–350 (this issue).
14. Cooper, L. Y., *Fire Safety Journal*, **16** (1990) 137.
15. Standard Guide for Room Fire Experiments, E 603-94, American Society for Testing and Materials. Philadelphia, PA, 15 July 1994, pp. 562–577.
16. Rasbash, D. J., *Transactions and Journal of the Plastics Institute*, Conference Supplement no. 2, 1967, pp. 55–62.